Biomaterials 33 (2012) 9009–9018

Contents lists available at SciVerse ScienceDirect

Biomaterials

journal homepage: www.elsevier.com/locate/biomaterials

Directed endothelial cell morphogenesis in micropatterned gelatin methacrylate hydrogels

Mehdi Nikkhah [a,b], Nouran Eshak [a,b], Pinar Zorlutuna [a,b], Nasim Annabi [a,b], Marco Castello [a,b], Keekyoung Kim [a,b], Alireza Dolatshahi-Pirouz [a,b], Faramarz Edalat [a,b], Hojae Bae [c], Yunzhi Yang [d], Ali Khademhosseini [a,b,e,*]

[a] Center for Biomedical Engineering, Department of Medicine, Brigham and Women's Hospital, Harvard Medical School, Boston, MA 02139, USA
[b] Harvard-MIT Division of Health Sciences and Technology, Massachusetts Institute of Technology, Cambridge, MA 02139, USA
[c] Department of Maxillofacial Biomedical Engineering and Institute of Oral Biology, School of Dentistry, Kyung Hee University, Seoul 130-701, Republic of Korea
[d] Department of Orthopaedic Surgery, School of Medicine, Stanford University, Stanford, CA 94305, USA
[e] Wyss Institute for Biologically Inspired Engineering, Harvard University, Cambridge, MA 02139, USA

ARTICLE INFO

Article history:
Received 16 August 2012
Accepted 29 August 2012
Available online 24 September 2012

Keywords:
Microfabrication
Hydrogel
Gelatin methacrylate
Endothelial cells
Cords

ABSTRACT

Engineering of organized vasculature is a crucial step in the development of functional and clinically relevant tissue constructs. A number of previous techniques have been proposed to spatially regulate the distribution of angiogenic biomolecules and vascular cells within biomaterial matrices to promote vascularization. Most of these approaches have been limited to two-dimensional (2D) micropatterned features or have resulted in formation of random vasculature within three-dimensional (3D) microenvironments. In this study, we investigate 3D endothelial cord formation within micropatterned gelatin methacrylate (GelMA) hydrogels with varying geometrical features (50–150 μm height). We demonstrated the significant dependence of endothelial cells proliferation, alignment and cord formation on geometrical dimensions of the patterned features. The cells were able to align and organize within the micropatterned constructs and assemble to form cord structures with organized actin fibers and circular/elliptical cross-sections. The inner layer of the cord structure was filled with gel showing that the micropatterned hydrogel constructs guided the assembly of endothelial cells into cord structures. Notably, the endothelial cords were retained within the hydrogel microconstructs for all geometries after two weeks of culture; however, only the 100 μm-high constructs provided the optimal microenvironment for the formation of circular and stable cord structures. Our findings suggest that endothelial cord formation is a preceding step to tubulogenesis and the proposed system can be used to develop organized vasculature for engineered tissue constructs.

© 2012 Elsevier Ltd. All rights reserved.

1. Introduction

Organ failure resulting from disease and trauma affects millions of Americans every year. Due to the limited availability of donors, transplantation has come to be only a partial solution. The field of tissue engineering has emerged to address this problem by generating transplantable tissues and organ substitutes [1–3]. Despite significant advances in this field, several challenges still remain towards developing fully functional engineered tissue constructs. Vascularization has been one of the major bottlenecks in tissue engineering [4–7]. In particular, most of the success in this field has come from creating thin and avascular tissues such as skin, cartilage and bladder. In contrast, larger and more complex tissues and organs require an adequate blood supply for the embedded cells within a tissue engineered construct. The critical importance of vascularization for sufficient oxygenation and nutrient delivery in complex tissues (*i.e.* heart, kidney, liver) has led researchers to develop new strategies to develop vasculature networks within engineered tissues. A number of these strategies, such as immobilization of angiogenic growth factors within a biomaterials matrix [8–11], are biomimetic attempts in which endothelial cells respond to angiogenic growth factors and ultimately migrate and assemble to form three-dimensional (3D) tubular structures. In cell-based approaches, a vascular bed is engineered throughout the construct by combining different types of vascular cells prior to implantation within a host [12–15].

* Corresponding author. Center for Biomedical Engineering, Department of Medicine, Brigham and Women's Hospital, Harvard Medical School, Boston, MA 02139, USA.
E-mail addresses: alik@rics.bwh.harvard.edu, alik@mit.edu (A. Khademhosseini).

0142-9612/$ – see front matter © 2012 Elsevier Ltd. All rights reserved.
http://dx.doi.org/10.1016/j.biomaterials.2012.08.068

It has been shown that the selection of appropriate biomaterials plays a crucial role in the formation of vascular network [16]. These scaffolds are required to provide a clinically suitable microenvironment to minimize cell loss and ensure rapid endothelial cell assembly and anastomoses with the host vasculature. Hydrogels are excellent biomaterials for tissue engineering applications mainly by providing a hydrated 3D microenvironment for homogenous cellular distribution, proper diffusion and mechanical properties and a structure that resembles the *in vivo* tissue architectures [17–19]. Hydrogels can be derived from natural sources such as collagen, fibrin, agarose, chitosan, and hyaluronic acid and can be used to deliver soluble growth factors or modified to form vascularized networks [17]. Alternatively, they can be synthesized by using synthetic materials such as poly(ethylene glycol)-diacrylate (PEGDA) [20,21].

To date, numerous studies have used hydrogels, as promising candidates, for vascularization applications. Some of these approaches have directly encapsulated vascular cells within hydrogel-based biomaterials to generate randomly distributed vasculature within the constructs [12,21]. Other approaches have utilized micro- and nanoscale technologies to develop highly organized microvessels and capillaries with precise geometrical features and distributions [22,23]. For instance, micropatterning techniques have been widely used to pattern multiple extracellular matrix (ECM) proteins (*i.e.* collagen, fibronectin) and synthetic materials such as PEGDA hydrogels in order to enhance endothelial cell alignment, morphogenesis and cord formation on two-dimensional (2D) surfaces [24–27]. Alternatively, a few studies have developed platforms to spatially control endothelial cell tubular formation in 3D scaffolds [28–31]. For instance, Raghavan *et al.* [28], have used micromolding technique to develop endothelial cell cord structures with variable geometrical features within collagen hydrogels. They were able to vary the diameter of the cord structures by changing the geometrical dimensions of the microchannels. However, so far there have not been detailed studies on role of hydrogel on 3D endothelial cell alignment and cord formation for long culture periods as a function of the microarchitecture.

In this paper, we present a simple, one-step microfabrication technique to create highly organized arrays of cell-laden GelMA hydrogel microconstructs to control endothelial cell organization, morphogenesis and cord formation. GelMA is an inexpensive and photocrosslinkable hydrogel, which can be subsequently patterned into desired features and geometrical dimensions. Notably, GelMA can be made with different degrees of methacrylation to modulate its biodegradability and mechanical robustness [32,33]. In this work, we micropatterned hydrogels with a high degree of methacrylation (low rate of biodegradability) with variable dimensions to investigate the process of endothelial cell cord formation for long culture periods. In addition, we studied endothelial cell proliferation, alignment and cord formation as a function of geometrical features of the hydrogel construct. The developed system may be used to fabricate organized vasculature within engineered tissue constructs and create platforms for drug and cytotoxicity studies as well as basic biological studies.

2. Materials and methods

2.1. Gelatin methacrylate synthesis

Methacrylated gelatin was synthesized as described previously [33]. Briefly, type A porcine skin gelatin was mixed at 10% (w/v) into Dulbecco's phosphate buffered saline (DPBS) (Sigma) at 60 °C and stirred until its components were fully dissolved. Subsequently, 8% (v/v) of methacrylic anhydride was added drop by drop to the gelatin solution and reacted at 50 °C for 3 h to form GelMA solutions. The solutions were then diluted and dialyzed against distilled water by using 12–14 kDa cutoff dialysis tubing water at 40 °C for one week. The solution was finally lyophilized for 4 days to produce white porous foam. The produced foam was stored at −80 °C for experimental use.

2.2. Cell culture preparation

Green fluorescent protein (GFP)-expressing human umbilical vein endothelial cells (HUVECs) were used in this study. The cells were maintained in physiological condition in 37 °C in a humidified, 5% CO_2-95% air atmosphere and cultured in T-75 flasks in endothelial cells basal medium (EBM-2; Lonza) supplemented with endothelial growth BulletKit (EGM-2; Lonza), 2% fetal bovine serum, vascular endothelial growth factor (VEGF), human fibroblast growth factor (hFGF), insulin growth factor (R3-IGF-I), human epidermal growth factor (hEGF), hydrocortisone, ascorbic acid, heparin, and 1% GA-1000 (gentamicin and amphotericin B). The media was changed twice per week and the cells were passaged once per week.

2.3. Microfabrication of patterned cell-laden GelMA hydrogel

Prior to cell encapsulation experiments, glass slides were treated with 3-(trimethoxysilyl)propyl methacrylate (TMSPMA) (Sigma) and then coated with a layer of 4.5% (w/v) poly(2-hydroxyethyl methacrylate) (PolyHEMA) (Sigma) solution in pure ethanol. The slides were then air dried for 3 days and sterilized by using UV light prior to encapsulation (Fig. 1A). GelMA prepolymer solution was prepared by dissolving 5% (w/v) GelMA macromers in PBS containing 0.5% (w/v) photoinitiator ((2-hydroxy-1-(4-(hydroxyethoxy) phenyl)-2-methyl-1-propanone), Irgacure 2959, CIBA Chemicals). The solution was then placed inside an 80 °C oven until it fully dissolved.

To prepare cell-laden micropatterned hydrogel constructs, HUVECs were trypsinized, counted and gently mixed in GelMA prepolymer solution with a final concentration of 2.5×10^7 cells/ml of GelMA solution. A 15 μl of prepolymer solution containing cells was then dropped on a petri dish in between the spacers with desirable height and a PolyHEMA-coated glass slide was inverted on the petri dish (Fig. 1B). Subsequently, the photomask layout (designed by AutoCAD software) was placed on top of the glass slide and the cell-encapsulated prepolymer solution was exposed to ultraviolet (UV) light (360–480 nm, 6.9 mW/cm^2 intensity) for 30 s to develop cell-laden micropatterned hydrogel constructs. Upon UV exposure, the polyHEMA-coated glass slides containing patterned, crosslinked hydrogel constructs were submerged into warm DPBS to develop the final hydrogel microconstructs (Fig. 1C). We used a 1 cm × 1 cm single photomaks layout to develop multiple parallel 8 mm-long by 50 μm-wide rectangular micropatterned constructs surrounded by a 1 mm-wide unpatterned region. Micropatterned GelMA constructs with different geometries were developed by changing the spacer height (H, 50, 100, 150 μm) (Fig. 1B). Following encapsulation, the microfabricated cell-laden hydrogel constructs were cultured in 24-well cell culture plates and supplemented with endothelial media for 1, 3 and 5 days prior to biological analyses.

2.4. Cell viability assay

Live/Dead Assay Kit (Invitrogen) that includes calcein AM (Cl) and ethidium homodimer (ETD) was used to quantify the percentage of viable cells after 1, 3, and 5 days of culture. A solution of 0.5 μl/ml Cl and 2 μl/ml ETD in DPBS were first prepared. The cell-laden GelMA gels were then rinsed with warm DPBS after which 200 μl of live/dead solution was added to each well. The well-plate was placed inside the incubator for 30 min and then imaged for live (green stain) and dead (red stain) cells using an inverted fluorescence microscope (Nikon TE 2000-U, Nikon instruments Inc., USA) with 10× magnifications. As HUVECs were expressing GFP, the total number of the cells (green stain) and the number of the dead cells stained with ETD, were counted within each image using ImageJ software (NIH). Then the number of the live cells was calculated by subtracting the number of the dead cells from the total number of the cells within each image. Finally, the cell viability was calculated based on the number of live cells divided by total cell number. At least three samples were prepared for each condition and three images were taken from each sample. The quantified values were reported based on the average ± standard deviation (SD).

2.5. Quantification of cell proliferation

Cell proliferation within the micropatterned and unpatterned regions was quantified by counting cellular nuclei over different culture times. To stain the nuclei of the cells that were encapsulated within hydrogels, the samples were rinsed in DPBS and fixed in 4% paraformaldehyde (PF) (Sigma) solution in DPBS. A 0.1% (v/v) DAPI (4′,6-diamidino-2-phenylindole) (Sigma) solution in DPBS was prepared and added to each sample. The samples were then placed inside the incubator for 10 min to stain the nuclei, after which the samples were washed three times in DPBS. The fluorescence images of the cells' nuclei were captured in 3–5 individual fields of micropatterned and unpatterned regions within each sample. The number of cell nuclei within each field was counted using NIH ImageJ software to assess the proliferation of HUVECs at different culture times (days 1, 3, and 5). At least three samples were stained for each condition.

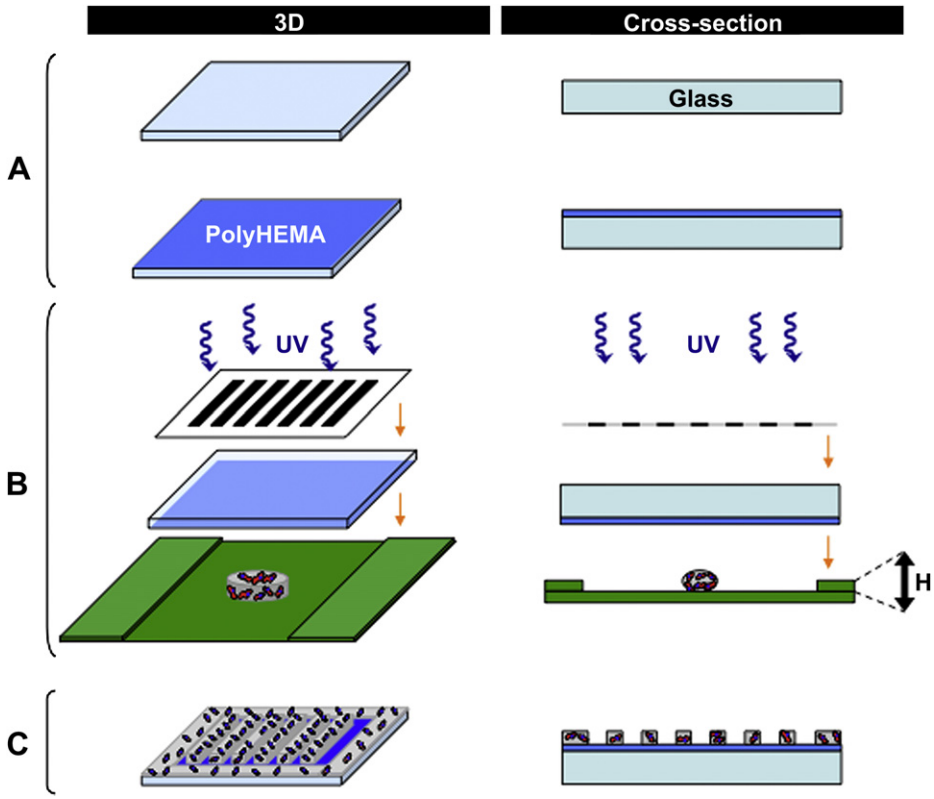

Fig. 1. Schematic drawing demonstrating the micropatterning procedure for generating endothelial cell-encapsulated GelMA hydrogels. (A) A glass substrate is initially coated with polyHEMA. (B) A drop of cell-encapsulated GelMA pre-polymer is poured on a petri dish in between the spacers of desired height (H) and the glass substrate is placed on top of the pre-polymer droplet. Then, UV light is focused on the droplet through a mask layout. (C) The rectangular microconstructs surrounded by an unpatterned region will be formed through washing the unexposed regions.

2.6. Quantification of cell alignment

After 5 days of culture, the samples were fixed in 4% PF solution in DPBS and the cells' nuclei were stained with DAPI as described previously. Alignment analysis was performed by using fluorescence images of DAPI-stained nuclei (3–5 images for each sample). The shape of individual nucleus within each image was fitted with an elliptical shape using built-in functions of ImageJ software. Then, the angles of the nuclei major elliptical axis with respect to the horizontal axis were defined as the cells nuclei alignment angles. Following measurement of individual nucleus alignment, all the nuclei alignment angles were normalized with respect to the average of all nuclei alignment within each image [32]. The normalized alignment angles were grouped in 10° increments to compare the nuclei alignment within patterned or unpatterned regions of each sample. Three samples were analyzed for each condition.

2.7. Immunofluorescence for cytoskeletal organization and angiogenic markers

Confocal microscopy was used to assess actin cytoskeleton organization, CD31 (PECAM-1), and VE-cadherein expression of cells encapsulated within the micropatterned regions of GelMA hydrogel constructs. The cell-laden GelMA gels were washed three times in DPBS and fixed in 4% PF solution in DPBS for 30 min. The samples were then soaked in 0.1% Triton X-100 in DPBS for 30 min to permeabilize the cells membrane. For actin cytoskeleton staining, the gels were blocked in 1% bovine serum albumin (BSA) in DPBS for 1 h. Then, a 1/40 dilution of Alexa Fluor-594 phalloidin (Invitrogen) in 0.1% BSA was added to the samples to stain the actin cytoskeleton following 45 min incubation at room temperature. For CD31 and VE-cadherin staining, upon fixation, the samples were blocked in 10% horse serum in DPBS for 1 h after cell fixation. To stain for CD31, a 1/100 dilution of monoclonal mouse anti-CD31 antibody (Abcam) in 10% horse serum was added to the cell-laden gels and the samples were kept at 4 °C for 24 h. The gels were then washed in DPBS three times with 1 h intervals in between the washing steps. After primary antibody staining, the samples were incubated in 1/200 dilution of Alexa Fluor-594 conjugated goat anti-mouse secondary antibody (Abcam) in 10% horse serum in DPBS for 6 h at room temperature (25 °C). Upon completion of staining, the samples were washed three times in DPBS. Similar procedure was used to stain VE-cadherin with the exception of using monoclonal rabbit anti-VE-cadherin antibody as the primary antibody and Alexa Fluor-594 conjugated goat anti-rabbit antibody as the secondary antibody. Following actin, CD31 and VE-cadherein staining, DAPI staining was also performed as described previously and the samples were mounted on Fluoromount-G solution (Southern Biotech) for confocal imaging.

Inverted laser scanning confocal microscope (SP5 X MP, Leica) and Leica application suite (LAS) software were used to acquire 3D serial section images of cord structures within GelMA hydrogels at different depths of foci. Diode laser (405 nm) and white light laser (470–670 nm) were used to image cell nuclei and actin, CD31 and VE-cadherin respectively. Acquired confocal images were stacked with Imaris software (Bitplane, Zurich, Swiss) to build the final 3D projected images.

2.8. Statistical analysis

Statistical significance was performed using one way analysis of variance (ANOVA) followed by Bonferroni's post-hoc test for multiple comparisons of different conditions using Graph Pad Prism 5.0 (San Diego, USA) statistical software. Data are presented as mean ± SD.

3. Results

3.1. Microfabrication of cell-laden GelMA hydrogel constructs with variable geometries

The micropatterned constructs were developed with 5% GelMA with high methacrylation degree (~70%) due to its mechanical robustness and suitability for micropatterning [33]. For the first experiment, we used 0.02% fluorescein dye to stain and visualize the GelMA hydrogel containing HUVECs on day 0 of culture. A cell-encapsulated micropatterned construct network surrounded by an unpatterned region was successfully formed upon UV exposure and hydrogel crosslinking process (Fig. 2A). Micropatterned constructs with different geometries were formed by changing the height of

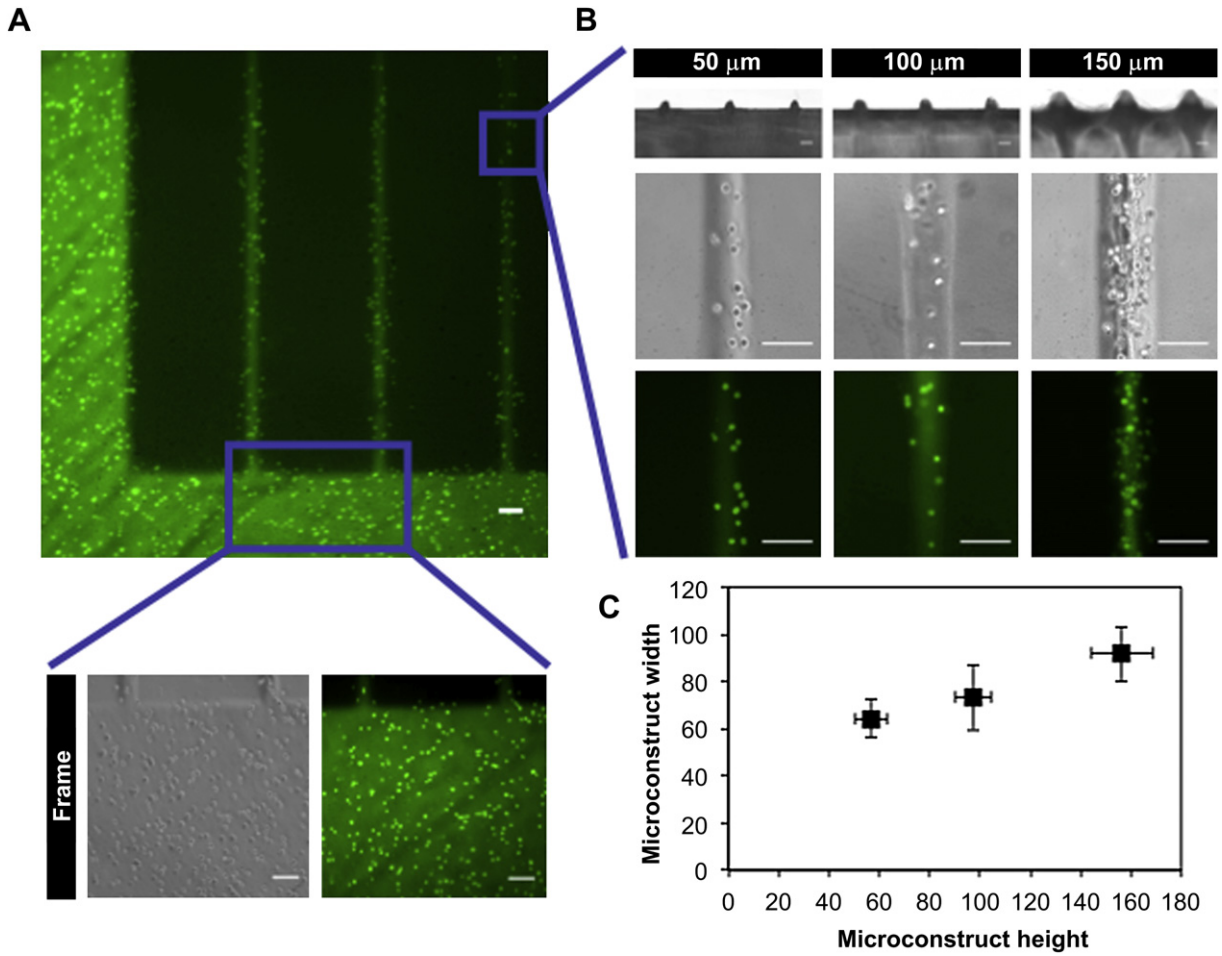

Fig. 2. Microfabricated cell-laden GelMA constructs comprised of microconstructs surrounded by an unpatterned region. (A) Phase contrast and fluorescence images of fluorescein-stained GelMA demonstrating the distribution of GFP-expressing HUVECs immediately after encapsulation. (B) Cross-sectional images of microconstructs with variable heights (50 μm, 100 μm, 150 μm). (C) Quantitative measurements demonstrating that microconstructs became wider by increasing the microconstructs height. Scale bars represent 100 μm.

the spacers (i.e. 50, 100, and 150 μm). The cross-sectional views of the fabricated microconstructs (Fig. 2B) demonstrated the formation of structures with rounded cross-sectional features due to UV light diffraction during the microfabrication process. Microconstruct widths and heights were measured using the phase contrast images. The height of cell-laden microconstructs were varied from 56.8 ± 6.6 μm ($n = 10$) to 97.3 ± 7.2 μm ($n = 17$) and 156.4 ± 12.4 μm ($n = 18$) when the spacer heights were changed from 50 μm to 100 μm and 150 μm, respectively. Despite using the same mask layout, the microconstruct width increased as a function of its height (Fig. 2C). Fluorescence and phase contrast images demonstrated successful cell encapsulation within microfabricated constructs of all the three different heights at day 0 of cell encapsulation. HUVECs were mostly round upon encapsulation and were homogeneously distributed within the 3D microenvironment of the hydrogel constructs. Overall, these data clearly indicated the formation of 3D cell-laden micropatterned hydrogel constructs with high fidelity and reproducibility.

3.2. Cell viability and proliferation within microfabricated GelMA constructs

We assessed viability and proliferation of HUVECs within micropatterned constructs as well as the unpatterned regions of GelMA hydrogels after 1, 3 and 5 days of culture. Cell viability was above 90% within the microconstructs for at least 5 days of culture. Interestingly, we detected a slight loss of cell viability as a function of hydrogel height and culture time within the unpatterned regions (Supplementary Figure S1). Overall, high cellular viability within the microconstructs indicated that the presence of photoinitiator in GelMA hydrogel along with the photolithography process (*i.e.* UV exposure) had minimal effect on endothelial cell survival.

Phase contrast and fluorescence images of GFP-expressing HUVECs demonstrated that the cells exhibited a rounded morphology on day 1 after cell encapsulation. However, after longer culture periods (days 3 and 5), interconnected networks of neighboring cells were formed within the hydrogel microconstructs (Fig. 3A). The cells remained within the micropatterned regions and did not migrate to the glass slide surface due to the cell-repellent properties of the polyHEMA coating. Within the micropatterned constructs, cells exhibited an elongated and spindle-like morphology and aligned along the direction of the microconstructs and formed organized networks with neighboring cells on day 5 of culture. Conversely, within the unpatterned regions, cells were randomly distributed within the 3D microenvironment of the hydrogel construct (Fig. 3A). Quantification of cell number within GelMA constructs demonstrated that the average cell number was significantly increased with culture time when the microconstruct height was less than 100 μm, demonstrating cellular proliferation within microconstructs with lower heights (Fig. 3B). However, there were no significant changes in cell number within the unpatterned regions of hydrogels (Fig. 3C).

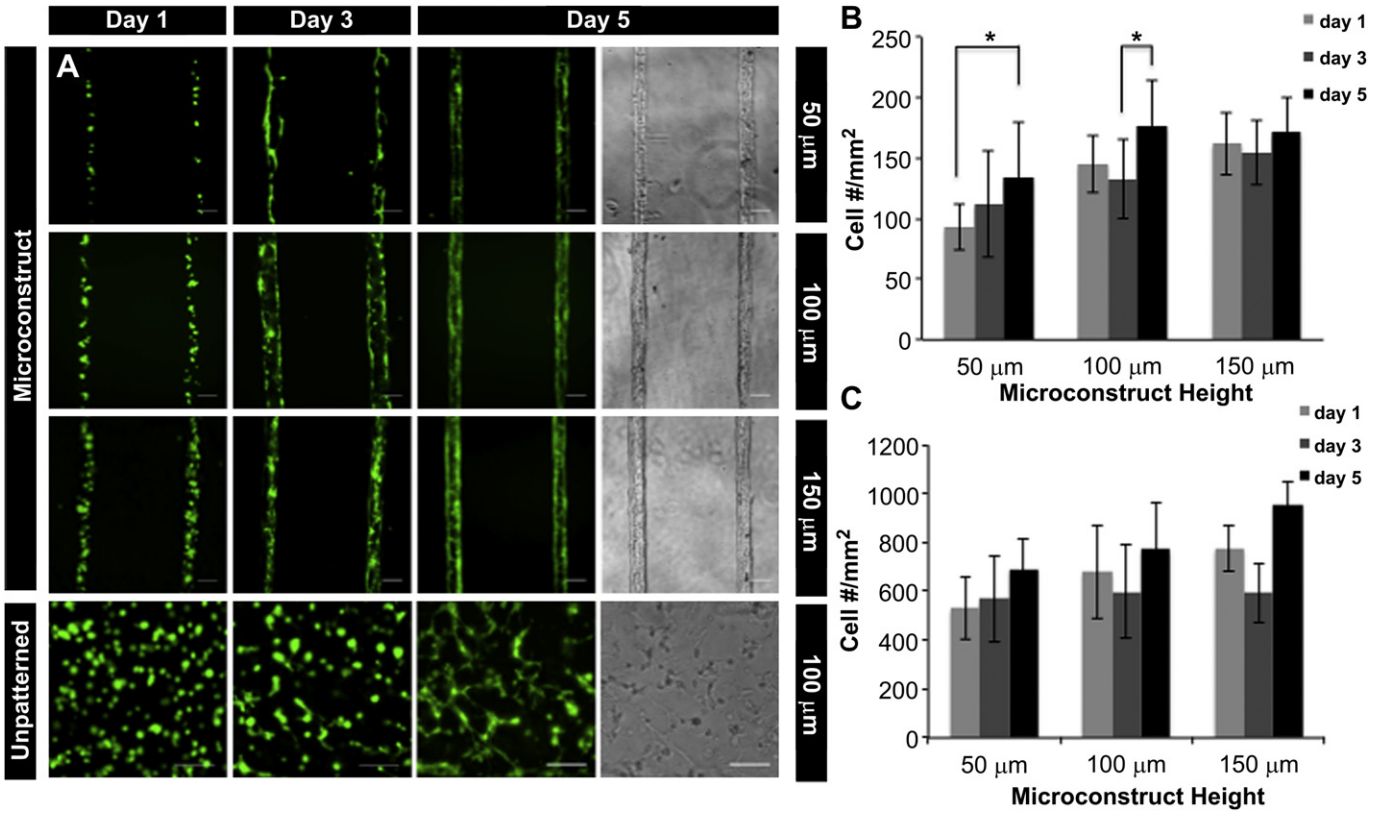

Fig. 3. (A) Representative fluorescence and phase contrast images showing GFP-expressing HUVECs encapsulated within micropatterned constructs and unpatterned regions of the GelMA hydrogels as a function of height and culture time. HUVEC proliferation was quantified within (B) Microconstructs and (C) Unpatterned regions of the hydrogel construct showing a significant increase in average cell number in 50 μm- and 100 μm-high microconstructs as a function of time. Data are presented in mean ± SD (*$p < 0.05$). Scale bars represent 100 μm.

3.3. Cellular alignment with micropatterned hydrogels

To assess the role of microconstructs geometries on cellular alignment, we quantified HUVECs nuclei alignment within patterned and unpatterned regions of the hydrogels as a function of construct height after 5 days of culture. Cells nuclei alignment was grouped in 10° increments to compare the alignment distribution in different conditions. As shown in Fig. 3A no alignment was observed within the micropatterned constructs on day 1 of encapsulation and nuclei alignment began after 3 days of encapsulation. On day 5 of culture, the cells filled the microconstructs and mostly aligned along the major axis of the microconstructs. In addition, we found dependence of cellular alignment on geometrical features of the patterns layout. As indicated in Fig. 4A–C, decreasing the height increased the percentage of nuclear alignment within the micropatterned constructs. For instance, in 50 μm- and 100 μm-high microconstructs, approximately 55% of the cells ($n = 389$, $n = 348$) aligned within the 0–10° increment angle, which was significantly higher than 39.9 ± 13.7% ($n = 453$) for 150 μm-high microconstructs ($p < 0.001$). In contrast to micropatterned regions, the cells nuclei were of randomly oriented within the unpatterned regions (Fig. 4D–F).

3.4. 3D cord formation of endothelial cells within micropatterned GelMA hydrogels

As shown previously (Fig. 3), HUVECs spread and aligned along the length of the microconstructs after 5 days of culture. The expressions of the endothelial cell specific markers including CD31 and VE-cadherin, as well as F-actin within the patterned regions were evaluated. We chose 100 μm-high constructs as a representative feature for the primary studies. Both CD31 and VE-cadherin are endothelial intercellular junctional proteins; CD31, also known as platelet endothelial cell adhesion molecule 1 (PECAM-1), makes up a large portion of endothelial cell intercellular junctions and is involved in angiogenesis [34,35]. Similarly, VE-cadherin is well known to have a substantial role in endothelial cell morphogenesis, angiogenesis, and vascular stability [36,37]. Confocal images of the cell-laden GelMA hydrogels revealed expression of CD31 and VE-cadherin within the micropatterned hydrogel constructs—an essential requirement to achieve a functional vasculature—only after 5 days of culture (Fig. 5A–D). The results of actin staining demonstrated that actin fibers aligned along the direction of the microconstructs. As shown in Fig. 5E–F, the cells reorganized within the hydrogel microconstructs to form cords with circular/elliptical cross sections (Arrows – Supplementary Movie M1). To study the role micropatterned hydrogel construct on endothelial cells cord formation, we repeated the experiments using FITC conjugated GelMA hydrogel. As shown in Fig. 6, confocal images revealed the presence of the hydrogel within the inner layer of cord structures after 5 days of culture (Arrows). The cells reorganized toward the outer surfaces and the periphery of the hydrogel construct to form cord structures. These observations indicate the significant role of patterned hydrogel microconstructs in guiding the assembly of endothelial cells toward cord formation.

To investigate the process of endothelial morphogenesis further within hydrogel constructs, we performed longer experiments (15 days) using samples of three different heights (50, 100 and 150 μm). Initially, the cells were immediately fixed upon encapsulation and imaged using confocal microscopy for GFP-expressing HUVECs. 3D

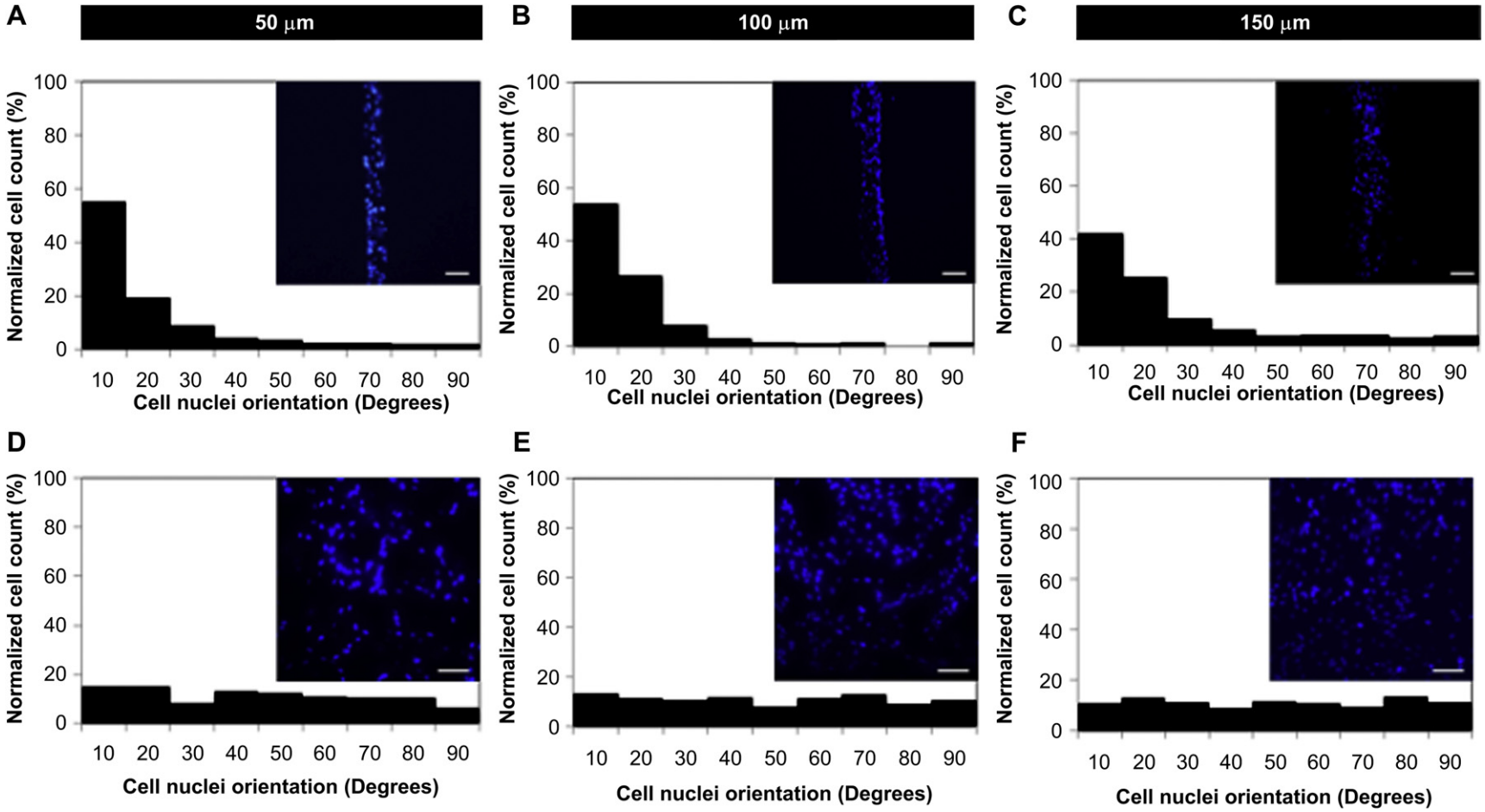

Fig. 4. Cells nuclei alignment within (A, B, C) microconstructs and (D, E, F) unpatterned regions of GelMA hydrogels as a function of height after 5 days of culture time. Representative fluorescence images demonstrate DAPI stained cells nuclei orientation within microconstructs and unpatterned regions of the hydrogel. Decreasing the height significantly enhanced HUVECs nuclei alignment within micropatterned constructs. Scale bars represent 100 μm.

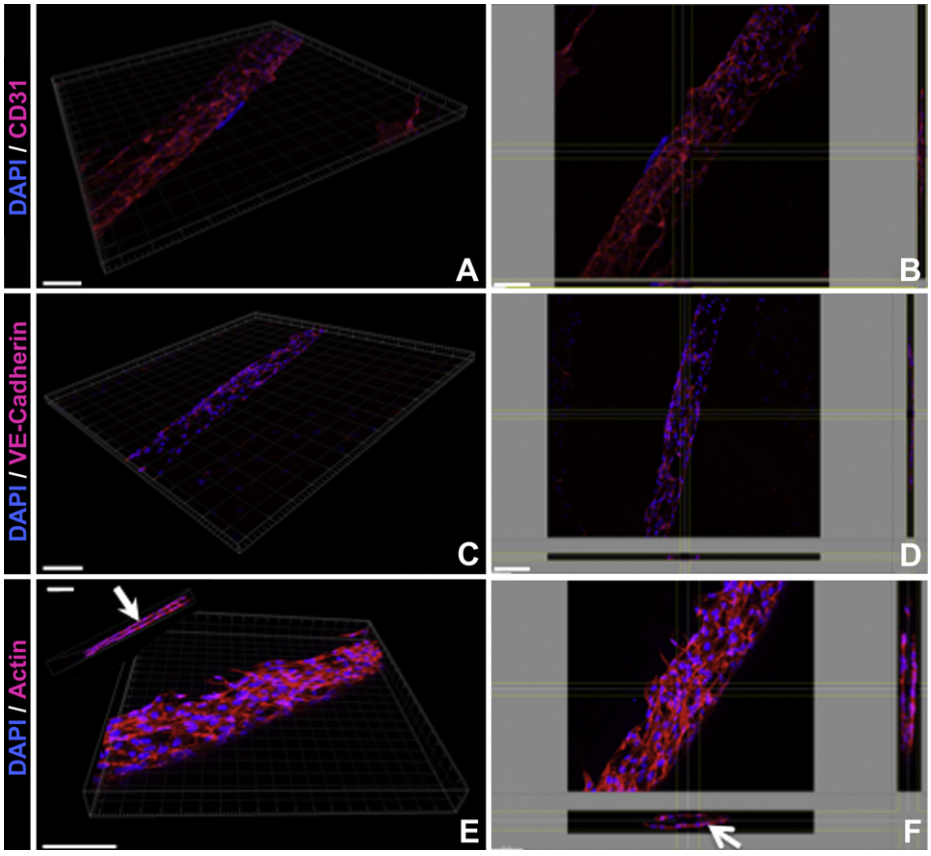

Fig. 5. Representative 3D and top view confocal images showing (A,B) CD31, (C,D) VE-cadherin and (E,F) actin cytoskeleton organization of HUVECs encapsulated within 100 μm-high microconstructs after 5 days of culture. Cross-sectional images in panel F demonstrate that HUVECs reorganized toward the periphery of the hydrogel constructs and self-assembled to form cord structures after 5 days of culture time. Scale bars represent 100 μm.

projected images illustrated that GFP-expressing HUVECs were comprised of round morphology and randomly distributed throughout the hydrogel layer for all the three different heights (Fig. 7A–F) consistent with our previous observation shown in Fig. 3. However, regardless of the height, confocal images demonstrated that the cells reorganized toward the periphery of the microconstructs, and formed stable cords after 15 days of culture (Fig. 7G–L). Interestingly, the cord structures were stable for two

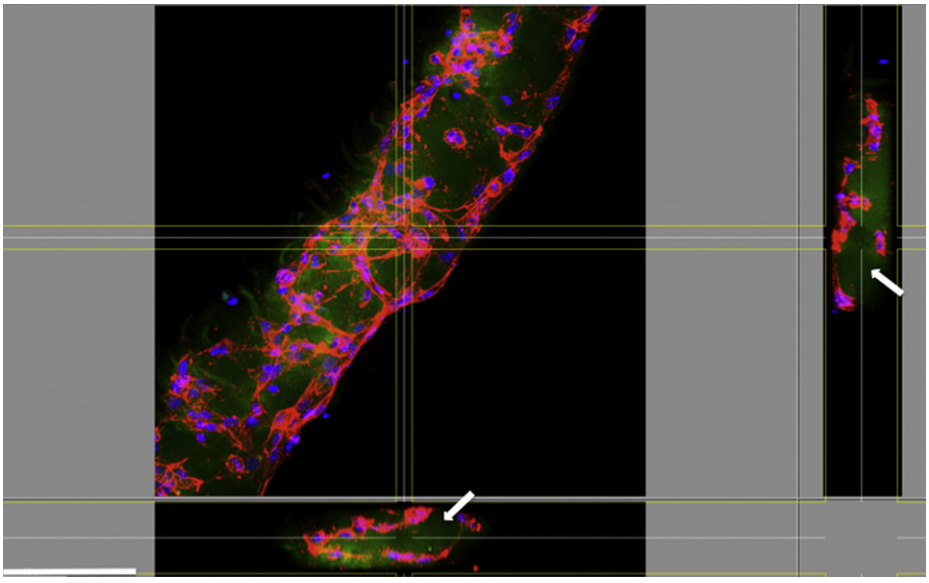

Fig. 6. Representative 3D confocal images of actin cytoskeleton organization of HUVECs encapsulated within FITC-conjugated 100 μm-high GelMA microconstructs. These images clearly demonstrate the presence of the gel (arrow) within the inner layer of the cord after 5 days of culture. Scale bar represents 100 μm.

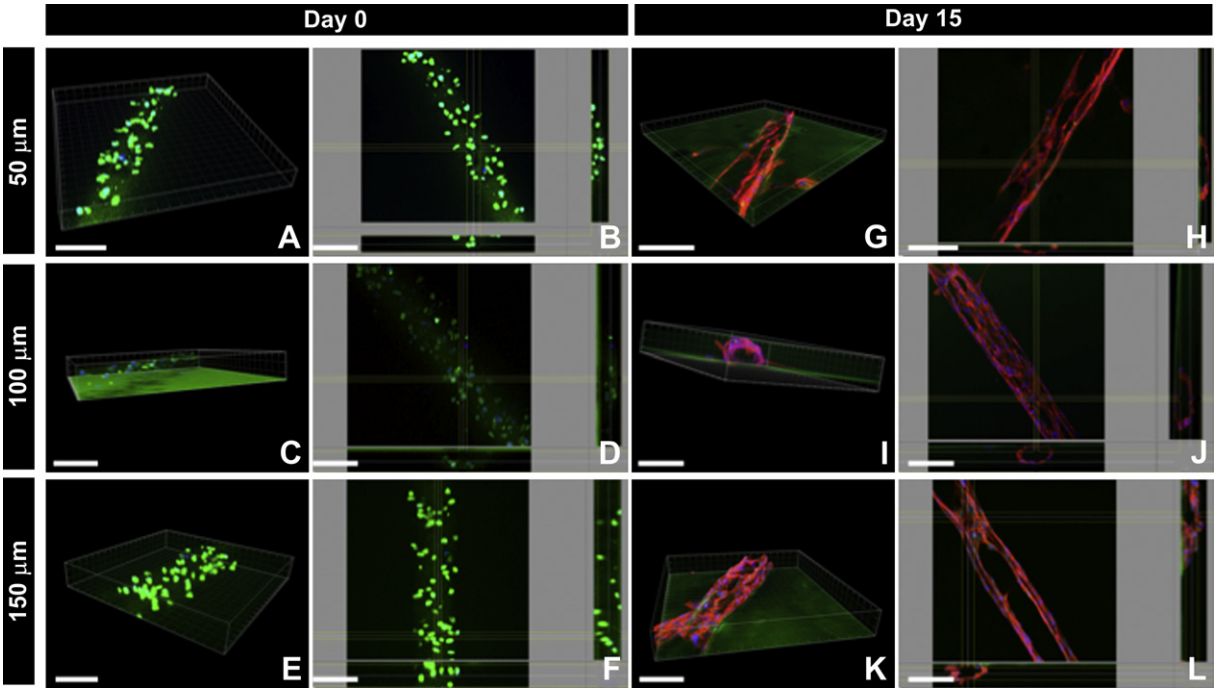

Fig. 7. Representative 3D and top view confocal images of (A–F) GFP-expressing and (G–L) DAPI/actin-stained HUVECs encapsulated within micropatterned GelMA hydrogel of varying heights demonstrating the process of cord formation after 15 days of culture. The cells were randomly distributed through the hydrogel layer at Day 0 of the culture, (A–F), while they reorganize toward the periphery of the micropatterned constructs to form cord structures for longer period of culture time (G–L). The cord structures were stable for 15 days of culture, while the 100 μm-high constructs provided the optimal microenvironment for the formation of cord structures with circular cross-section (I,J). Scale bars represent 100 μm.

weeks of culture time. Specifically, for the 50 μm-high microconstructs, the cross-section of the cord structure resembled a semi-elliptical shape (Fig. 7G and H), while cords of the 100 μm-high microconstructs comprised a more circular cross-section (Fig. 7I and J). Although the cord structures were retained inside 150 μm-high microconstructs, the cells were poorly organized compared to 50 μm and 100 μm-high micropatterned constructs (Fig. 7K and L). Notably, confocal images clearly demonstrated that the actin fibers were distributed in a more organized fashion within the 100 μm-high micropatterned hydrogel constructs compared to the other geometrical features (*i.e.* 50 μm and 150 μm). These data suggest that 100 μm-high constructs provide the optimal microenvironment in terms of geometrical feature for the formation of circular and stable cords.

4. Discussion

The development of functional vasculature remains one of the major challenges in tissue engineering [4,6]. In the past few years, numerous strategies have been developed to engineer vascularized networks within engineered tissue constructs. Some of these strategies have exploited cell-based approaches in which vascular cells have been embedded within scaffolds to reorganize and form capillary networks [12–15]. For instance, our group previously demonstrated that the co-culture of endothelial cells with mesenchymal stem cells (MSCs) significantly enhanced the formation of stable capillaries within a bulk GelMA hydrogel [12]. These approaches have usually resulted in the formation of randomly distributed capillaries within the hydrogel construct. Other approaches have used 2D micropatterning and micromolding techniques to create highly organized endothelial cell cord and tubular structures [24–28,30]. However, only a limited number of studies have investigated the process of endothelial cord formation within the 3D architecture of hydrogel microconstructs.

In this work, we used microfabrication techniques to create highly organized endothelial cord structures in a cell-laden hydrogel consisting of microconstructs with variable geometries to enhance endothelial cell alignment and morphogenesis. We used GelMA as a suitable biomaterial to conduct our study. GelMA is a non-cytotoxic and biodegradable polymer that is modified with methacrylate groups to render it photocrosslinkable rendering it amenable to microfabrication techniques (*i.e.* photolithography) [33,38]. GelMA has attracted significant attention in tissue engineering and stem cell bioengineering mainly by retaining cell binding motifs and mechanical robustness. In this study, encapsulation of HUVECs within the micropatterned GelMA hydrogels with high degrees of methacrylation resulted in high cellular viability and alignment along the direction of the microconstructs. This was in agreement with our previous work conducted on fibroblastic cells showing that 64 ± 8% of the cells encapsulated within 50 μm-wide micropatterned GelMA hydrogels were elongated and aligned along the direction of the micropatterned features [32]. We found that the degree of cell alignment within the patterned hydrogel was enhanced by decreasing the pattern height. The cells established mature intercellular junctions, detected through visualization of CD31 and VE-cadherein proteins after 5 days in culture, and formed stable cords with circular/elliptical cross-sections in micropatterned hydrogel constructs. Although the average cell number was significantly increased in 50 μm- and 100 μm-high microconstructs, the cell proliferation was not significantly different within the unpatterned regions of the hydrogel as a function of time. We observed similar behavior for endothelial colony forming cells (ECFC) within GelMA hydrogels of varying methacrylation degrees [12]. This behavior is expected subsequent to cell–cell adhesion, initiated as early as 3 days of culture time, and may be due to contact inhibition of cells.

Supplementary video related to this article can be found at http://dx.doi.org/10.1016/j.biomaterials.2012.08.068.

A critical aspect of our finding was the formation of stable endothelial cord structures comprised of circular/elliptical cross-sections with highly organized actin fibers as early as 5 days of culture. Although the architecture of the endothelial structures resembled tubules, we observed upon cross-sectional imaging that the cords were filled with gel. Previous studies have demonstrated that vascularization and capillary morphogenesis are 3D, matrix-specific processes, highly dependent on the composition and properties of biomaterial matrix along with the presence of angiogenic growth factors [39–44]. For instance, several studies have demonstrated that endothelial cells embedded within Matrigel or collagen gels were able to form networks of branching capillary tubes containing a patent lumen [39,45–47]. When cells are seeded or encapsulated within a flexible hydrogel substrate (*i.e.* collagen I), they bind to the substrate matrix via integrins, form focal adhesion complexes, undergo morphogenesis, and generate traction forces. In this process, each cell is a localized center for the generated traction force field [47–49]. Such behavior consequently remodels the ECM (*i.e.* collagen fibers) and results in migration, cytoskeletal reorganization and assembly of neighboring endothelial cells into networks of cords and tubular structures [42]. Other studies have demonstrated that when endothelial cells are patterned on predefined geometrical features (*i.e.* circular patterns), they exert traction forces and generate a mechanical stress profile, with higher stress concentrated on the periphery of the features [50].

The advantages of using GelMA hydrogels in this work are provision of a flexible substrate and presence of cell binding motifs to support endothelial cell cord formation. Initially, on day 0 of culture, the endothelial cells exhibit round morphology and are mostly embedded within the gel constructs with only a few cells located on the outer surface of the hydrogel construct. Upon cell spreading within the micropatterned constructs, they align along the major axis of the microconstructs with highly organized and oriented actin fibers. Simultaneously, the cells spread to reach their neighboring cells, form cell–cell junctions and exert 3D traction forces along the direction of the patterned microconstructs due to the geometrical confinement within the microconstructs. Formation of cell–cell junctions between the cells in the periphery and within the gel and the resultant traction forces generated by actin cytoskeletal fibers [42,51] directs the assembly of cells toward the outer surface of the hydrogel construct. Cell–cell junctions between endothelial cells are believed to play a crucial role in transmission of contractile stresses [52] and generation of a mechanically-equilibrated structure (*i.e.* cords). This is not the case for other cell types as a previous study revealed the absence of cord-like structures using fibroblastic cells within micropatterned GelMA hydrogel constructs with similar geometrical features compared to the present study [32]. Additionally, the higher proliferation of cells within 50- and 100 μm-high microconstructs compared to the unpatterned and 150 μm-high features, is expected to be due to the enhanced organization of the cells and generation of higher contractile stresses concentrated on the outer surface of the patterned microconstructs [50].

Based on our findings, it is believed that the micropatterned hydrogel constructs guides the assembly of the endothelial cells toward formation of relatively large cord structures (50–150 μm diameter) in a contractile stress dependent manner in the presence of angiogenic growth factors (*i.e.* VEGF and bFGF) [40,53–55]. Such mechanism is different compared to the formation of smaller tubular structures and capillaries (5–10 μm) where endothelial cell polarization, intracellular vacuoles and recruitment of mural cells initiate the process of tubulogenesis [12,21]. Therefore, we expect that in the presence of relatively large-diameter hydrogel constructs (~100 μm), the assembly of endothelial cells is a preceding step to development of tubules, while the co-culture of mural cells with endothelial cells will result in faster degradation of the gel and formation of lumens.

The findings of this work are in agreement with previous studies in terms of cellular alignment and cord formation [26–28]. In a recent study, Raghavan *et al.* embedded endothelial cell-laden collagen hydrogels within a polydimethylsiloxane (PDMS) micromold and demonstrated that the cells were able to undergo morphogenesis and self-assemble to form cords in response to bFGF and VEGF stimulation [28]. However, our work demonstrates the suitability of GelMA hydrogels in providing a permissive 3D microenvironment for cell adhesion, migration and formation of stable and organized cord structures with variable sizes and features for a long period of culture time. In addition, our approach does not require conjugation of cell adhesion ligands and angiogenic factors within hydrogel constructs and our microfabrication technique is a simple, one step-process without the need for any prefabricated micromold to develop and maintain stable cord structures. Future attempts can be focused on development of more biomimetic vasculature within the patterned hydrogel constructs through co-culturing of endothelial cells with mural cells.

5. Conclusion

In this study, we used a microfabrication technique (*i.e.* photolithography) to create highly organized endothelial cord structures comprised of circular/elliptical cross-sections using GelMA hydrogels. The cells encapsulated within the 3D hydrogels exhibited high expression of endothelial cell specific makers and formed cord structures with highly organized actin fibers only after 5 days of culture. By varying the geometrical features of the microconstructs, it was possible to optimize the formation of stable cords for more than two weeks. The presented findings introduce a promising approach for merging microfabrication technologies and biomaterials to develop 3D organized vascularized networks for tissue engineering applications.

Acknowledgments

The authors acknowledge funding from the National Science Foundation CAREER Award (DMR 0847287), the office of Naval Research Young National Investigator Award, and the National Institutes of Health (HL092836, DE019024, EB012597, AR057837, DE021468, HL099073).

Appendix A. Supplementary data

Supplementary data related to this article can be found at http://dx.doi.org/10.1016/j.biomaterials.2012.08.068.

References

[1] Langer R, Vacanti JP. Tissue engineering. Science 1993;260:920–6.
[2] Khademhosseini A, Langer R. Microengineered hydrogels for tissue engineering. Biomaterials 2007;28:5087–92.
[3] Griffith LG, Naughton G. Tissue engineering - current challenges and expanding opportunities. Science 2002;295:1009–14.
[4] Lovett M, Lee K, Edwards A, Kaplan DL. Vascularization strategies for tissue engineering. Tissue Eng Part B Rev 2009;15:353–70.
[5] Kaully T, Kaufman-Francis K, Lesman A, Levenberg S. Vascularization-the conduit to viable engineered tissues. Tissue Eng Part B Rev 2009;15:159–69.
[6] Moon JJ, West JL. Vascularization of engineered tissues: approaches to promote angiogenesis in biomaterials. Curr Top Med Chem 2008;8:300–10.
[7] Niklason LE, Langer RS. Advances in tissue engineering of blood vessels and other tissues. Transpl Immunol 1997;5:303–6.
[8] Lee H, Cusick RA, Browne F, Kim TH, Ma PX, Utsunomiya H, et al. Local delivery of basic fibroblast growth factor increases both angiogenesis and engraftment of hepatocytes in tissue-engineered polymer devices. Transplantation 2002; 73:1589–93.

[9] Lee KY, Peters MC, Anderson KW, Mooney DJ. Controlled growth factor release from synthetic extracellular matrices. Nature 2000;408:998–1000.
[10] Chen RR, Silva EA, Yuen WW, Mooney DJ. Spatio-temporal VEGF and PDGF delivery patterns blood vessel formation and maturation. Pharm Res 2007;24:258–64.
[11] Isner JM, Pieczek A, Schainfeld R, Blair R, Haley L, Asahara T, et al. Clinical evidence of angiogenesis after arterial gene transfer of phVEGF(165) in patient with ischaemic limb. Lancet 1996;348:370–4.
[12] Chen Y, Lin RZ, Qi H, Yang Y, Bae H, Melero-Martin JM, et al. Functional human vascular network generated in photocrosslinkable gelatin methacrylate hydrogels. Adv Funct Mater 2012;22:2027–39.
[13] Koike N, Fukumura D, Gralla O, Au P, Schechner JS, Jain RK. Creation of long-lasting blood vessels. Nature 2004;428:138–9.
[14] Melero-Martin JM, De Obaldia ME, Kang S-Y, Khan ZA, Yuan L, Oettgen P, et al. Engineering robust and functional vascular networks in vivo with human adult and cord blood-derived progenitor cells. Circ Res 2008;103:194–202.
[15] Traktuev DO, Prater DN, Merfeld-Clauss S, Sanjeevaiah AR, Saadatzadeh MR, Murphy M, et al. Robust functional vascular network formation in vivo by cooperation of adipose progenitor and endothelial cells. Circ Res 2009;104:1410–20.
[16] Shastri VP. In vivo engineering of tissues: biological considerations, challenges, strategies, and future directions. Adv Mater 2009;21:3246–54.
[17] Lee KY, Mooney DJ. Hydrogels for tissue engineering. Chem Rev 2001;101:1869–79.
[18] Slaughter BV, Khurshid SS, Fisher OZ, Khademhosseini A, Peppas NA. Hydrogels in regenerative medicine. Adv Mater 2009;21:3307–29.
[19] Peppas NA, Hilt JZ, Khademhosseini A, Langer R. Hydrogels in biology and medicine: from molecular principles to bionanotechnology. Adv Mater 2006;18:1345–60.
[20] Leslie-Barbick JE, Moon JJ, West JL. Covalently-immobilized vascular endothelial growth factor promotes endothelial cell tubulogenesis in poly(ethylene glycol) diacrylate hydrogels. J Biomater Sci Polym Ed 2009;20:1763–79.
[21] Moon JJ, Saik JE, Poche RA, Leslie-Barbick JE, Lee S-H, Smith AA, et al. Biomimetic hydrogels with pro-angiogenic properties. Biomaterials 2010;31:3840–7.
[22] Andersson H, van den Berg A. Microfabrication and microfluidics for tissue engineering: state of the art and future opportunities. Lab Chip 2004;4:98–103.
[23] Zorlutuna P, Annabi N, Camci-Unal G, Nikkhah M, Cha JM, Nichol JW, et al. Microfabricated biomaterials for engineering 3D tissues. Adv Mater 2012;24:1782–804.
[24] Dike LE, Chen CS, Mrksich M, Tien J, Whitesides GM, Ingber DE. Geometric control of switching between growth, apoptosis, and differentiation during angiogenesis using micropatterned substrates. In Vitro Cell Dev Biol Anim 1999;35:441–8.
[25] Moon JJ, Hahn MS, Kim I, Nsiah BA, West JL. Micropatterning of poly(ethylene glycol) diacrylate hydrogels with biomolecules to regulate and guide endothelial morphogenesis. Tissue Eng Part A 2009;15:579–85.
[26] Dickinson LE, Moura ME, Gerecht S. Guiding endothelial progenitor cell tube formation using patterned fibronectin surfaces. Soft Matter 2010;6:5109–19.
[27] Leslie-Barbick JE, Shen C, Chen C, West JL. Micron-scale spatially patterned, covalently immobilized vascular endothelial growth factor on hydrogels accelerates endothelial tubulogenesis and increases cellular angiogenic responses. Tissue Eng Part A 2011;17:221–9.
[28] Raghavan S, Nelson CM, Baranski JD, Lim E, Chen CS. Geometrically controlled endothelial tubulogenesis in micropatterned gels. Tissue Eng Part A 2010;16:2255–63.
[29] Chrobak KM, Potter DR, Tien J. Formation of perfused, functional microvascular tubes in vitro. Microvasc Res 2006;71:185–96.
[30] Zheng Y, Chen J, Craven M, Choi NW, Totorica S, Diaz-Santana A, et al. In vitro microvessels for the study of angiogenesis and thrombosis. Proc Natl Acad Sci U S A 2012;109:9342–7.
[31] Sadr N, Zhu M, Osaki T, Kakegawa T, Yang Y, Moretti M, et al. SAM-based cell transfer to photopatterned hydrogels for microengineering vascular-like structures. Biomaterials 2011;32:7479–90.
[32] Aubin H, Nichol JW, Hutson CB, Bae H, Sieminski AL, Cropek DM, et al. Directed 3D cell alignment and elongation in microengineered hydrogels. Biomaterials 2010;31:6941–51.
[33] Nichol JW, Koshy ST, Bae H, Hwang CM, Yamanlar S, Khademhosseini A. Cell-laden microengineered gelatin methacrylate hydrogels. Biomaterials 2010;31:5536–44.
[34] Albelda SM, Muller WA, Buck CA, Newman PJ. Molecular and cellular properties of pecam-1 (endocam/cd31) - a novel vascular cell cell-adhesion molecule. J Cell Biol 1991;114:1059–68.
[35] DeLisser HM, Christofidou–Solomidou M, Strieter RM, Burdick MD, Robinson CS, Wexler RS, et al. Involvement of endothelial PECAM-1/CD31 in angiogenesis. Am J Pathol 1997;151:671–7.
[36] Bach TL, Barsigian C, Chalupowicz DG, Busler D, Yaen CH, Grant DS, et al. VE-cadherin mediates endothelial cell capillary tube formation in fibrin and collagen gels. Exp Cell Res 1998;238:324–34.
[37] Vestweber D. VE-cadherin - the major endothelial adhesion molecule controlling cellular junctions and blood vessel formation. Arterioscler Thromb Vasc Biol 2008;28:223–32.
[38] Van den Bulcke AI, Bogdanov B, De Rooze N, Schacht EH, Cornelissen M, Berghmans H. Structural and rheological properties of methacrylamide modified gelatin hydrogels. Biomacromolecules 2000;1:31–8.
[39] Montesano R, Orci L, Vassalli P. Invitro rapid organization of endothelial-cells into capillary-like networks is promoted by collagen matrices. J Cell Biol 1983;97:1648–52.
[40] Jackson CJ, Jenkins KL. Type-I collagen fibrils promote rapid vascular tube formation upon contact with the apical side of cultured endothelium. Exp Cell Res 1991;192:319–23.
[41] Madri JA, Williams SK. Capillary endothelial cell-cultures - phenotypic modulation by matrix components. J Cell Biol 1983;97:153–65.
[42] Vernon RB, Lara SL, Drake CJ, Iruela-Arispe ML, Angello JC, Little CD, et al. Organized type-I collagen influences endothelial patterns during spontaneous angiogenesis in vitro - planar cultures as models of vascular development. In Vitro Cell Dev Biol Anim 1995;31:120–31.
[43] Ingber DE, Folkman J. How does extracellular-matrix control capillary morphogenesis. Cell 1989;58:803–5.
[44] Ghajar CM, Chen X, Harris JW, Suresh V, Hughes CCW, Jeon NL, et al. The effect of matrix density on the regulation of 3-D capillary morphogenesis. Biophys J 2008;94:1930–41.
[45] Allen P, Melero-Martin JM, Bischoff J. Type I collagen, fibrin and PuraMatrix matrices provide permissive environments for human endothelial and mesenchymal progenitor cells to form neovascular networks. J Tissue Eng Regen Med 2011;5:E74–86.
[46] Davis GE, Senger DR. Endothelial extracellular matrix - biosynthesis, remodeling, and functions during vascular morphogenesis and neovessel stabilization. Circ Res 2005;97:1093–107.
[47] Vernon RB, Sage EH. Between molecules and morphology - extracellular-matrix and creation of vascular form. Am J Pathol 1995;147:873–83.
[48] Manoussaki D, Lubkin SR, Vernon RB, Murray JD. A mechanical model for the formation of vascular networks in vitro. Acta Biotheor 1996;44:271–82.
[49] Davis GE, Camarillo CW. An alpha 2 beta 1 integrin-dependent pinocytic mechanism involving intracellular vacuole formation and coalescence regulates capillary lumen and tube formation in three-dimensional collagen matrix. Exp Cell Res 1996;224:39–51.
[50] Nelson CM, Jean RP, Tan JL, Liu WF, Sniadecki NJ, Spector AA, et al. Emergent patterns of growth controlled by multicellular form and mechanics. Proc Natl Acad Sci U S A 2005;102:11594–9.
[51] Kniazeva E, Putnam AJ. Endothelial cell traction and ECM density influence both capillary morphogenesis and maintenance in 3-D. Am J Physiol Cell Physiol 2009;297:C179–87.
[52] Gjorevski N, Nelson CM. Endogenous patterns of mechanical stress are required for branching morphogenesis. Integr Biol 2010;2:424–34.
[53] Huang JZ, Frischer JS, Serur A, Kadenhe A, Yokoi A, McCrudden KW, et al. Regression of established tumors and metastases by potent vascular endothelial growth factor blockade. Proc Natl Acad Sci U S A 2003;100:7785–90.
[54] Inai T, Mancuso M, Hashizume H, Baffert F, Haskell A, Baluk P, et al. Inhibition of vascular endothelial growth factor (VEGF) signaling in cancer causes loss of endothelial fenestrations, regression of tumor vessels, and appearance of basement membrane ghosts. Am J Pathol 2004;165:35–52.
[55] Yuan F, Chen Y, Dellian M, Safabakhsh N, Ferrara N, Jain RK. Time-dependent vascular regression and permeability changes in established human tumor xenografts induced by an anti-vascular endothelial growth factor vascular permeability factor antibody. Proc Natl Acad Sci U S A 1996;93:14765–70.